Update analysis of $\psi(3686) \to p\bar{p}$*

Zhi Gao (高枝)[1†] Rong-Gang Ping (平荣刚)[2,3‡] Minggang Zhao (赵明刚)[1§]

[1]Nankai University, Tianjin 300071, China
[2]Institute of High Energy Physics, Chinese Academy of Sciences, Beijing 100049, China
[3]University of Chinese Academy of Sciences, Beijing 100049, China

Abstract: We have performed an updated analysis of the angular distribution of the $\psi(3686) \to p\bar{p}$ decay by considering transverse beam polarization to investigate potential sources of forward-backward asymmetry and azimuthal modulation beyond the simple $1+\alpha\cos^2\theta$ form. We focus on the interference between the $\psi(3686)$ resonance and two-photon exchange continuum process, as well as on the background from initial-state–final-state radiation (ISR–FSR) interference. A maximum-likelihood fit to the $\cos\theta$ distribution of $\psi(3686) \to p\bar{p}$ yields $\alpha = 1.00 \pm 0.03$, which is consistent with previous results. Our model predicts a significant $\sin(2\phi)$ modulation in the azimuthal angle, indicating the influence of transverse beam polarization. Based on these findings, two-dimensional angular analyses can be conducted in the future to fully disentangle the polarization and interference dynamics in charmonium decays to baryon pairs.

Keywords: transverse beam polarization, forward-backward asymmetry, electron–positron collider

DOI: 10.1088/1674-1137/ae4a0c **CSTR:** 32044.14.ChinesePhysicsC.50063002

I. INTRODUCTION

Precise measurements of the electromagnetic form factors of nucleons in the timelike region through processes such as $e^+e^- \to p\bar{p}$ and $e^+e^- \to n\bar{n}$ provide crucial insights into the non-perturbative structure of baryons. These form factors, encoding the spatial distributions of electric charge and magnetization, serve as fundamental probes of Quantum Chromodynamics (QCD) in the confinement regime. The data obtained from the BESIII experiment [1–3], with unprecedented precision, enable stringent tests of theoretical models and help resolve long-standing puzzles, such as the relative strength of photon couplings to protons and neutrons and the oscillatory behavior [4–5] observed in the effective form factors. Such studies bridge the spacelike and timelike domains, offering deeper insights into nucleon dynamics, the role of final-state interactions, and the transition between perturbative and non-perturbative QCD.

The differential cross-section for the annihilation process $e^+e^- \to B\bar{B}$, where B denotes a proton (p) or neutron (n), is expressed as a function of the center-of-mass energy squared (s) and the polar angle (θ) of the baryon:

$$\frac{\mathrm{d}\sigma_B(s)}{\mathrm{d}\Omega} = \frac{\alpha_{\mathrm{QED}}^2\beta C}{4s}\left[|G_M(s)|^2(1+\cos^2\theta) + \frac{4m_B^2}{s}|G_E(s)|^2\sin^2\theta\right], \tag{1}$$

where α_{QED} is the fine-structure constant, $\beta = \sqrt{1-4m_B^2/s}$ is the baryon velocity, m_B is the baryon mass, and C is the Coulomb enhancement factor for the charged final states ($p\bar{p}$) or is unity for the neutral ones ($n\bar{n}$). The electric and magnetic Sachs form factors $G_E(s)$ and $G_M(s)$ characterize the internal spatial distributions of charge and magnetization, respectively. Their ratio $|G_E/G_M|$ and individual moduli can be extracted by fitting the measured $\cos\theta$ distributions. In the timelike region ($s > 0$), these form factors are complex, and their behavior near the threshold provides critical information on final-state interactions and non-perturbative QCD dynamics

The angular distributions in the $J/\psi \to p\bar{p}$ and $n\bar{n}$ decays, parameterized as $1+\alpha\cos^2\theta$, serve as sensitive probes of the underlying baryon structure and production dynamics [6–8]. These decays proceed via three-gluon annihilation, offering a gluon-rich environment to test perturbative QCD and determine the role of gluon spin. The parameter α reflects the interplay among quark-mass

Received 6 January 2026; Accepted 25 February 2026; Accepted manuscript online 26 February 2026

* The work is partly supported by the National Natural Science Foundation of China(NSFC) (12575112)

† E-mail: zhi-gao@mail.nankai.edu.cn
‡ E-mail: pingrg@ihep.ac.cn
§ E-mail: zhaomg@nankai.edu.cn

effects, relativistic corrections, and baryon wave functions, distinguishing between asymptotic predictions and non-perturbative models. Measurements of α for both the $p\bar{p}$ and $n\bar{n}$ final states can reveal isospin dependencies and $SU(3)$ flavor-symmetry breaking, and comparisons with $\psi(3686)$ decays can be performed to test heavy-quark spin symmetry and production mechanisms. Such studies are crucial for constraining quark models, understanding baryon formation, and exploring exotic hadronic configurations.

The data obtained by measuring α in the $p\bar{p}$ and $n\bar{n}$ channels in BES, BESIII, and CLEO experiments are summarized in Table 1. Existing data, primarily obtained from BES and CLEO experiments, reveal that the measured $\alpha_{p\bar{p}}$ for $\psi(3686)$ is approximately 1.03 ± 0.07 [9], which has been obtained consistently and is larger than the J/ψ value of 0.676 ± 0.055 [10], suggesting different dynamical origins. The first observation of $\psi(3686)\to n\bar{n}$ by BESIII yielded $\alpha_{n\bar{n}}=0.68\pm0.16$ [9], which was consistent with $\alpha_{p\bar{p}}$ measured in J/ψ decays within one standard deviation; however, the discrepancy in this value is greater than 1σ compared to that obtained from $\psi(3686)$ decays. The considerable uncertainties preclude definitive conclusions, thus motivating further precision studies to understand flavor-symmetry breaking and the role of quark-mass effects in charmonium decays to baryon pairs.

The measured branching ratios for $\psi(3686)\to p\bar{p}$ and $\psi(3686)\to n\bar{n}$ are consistent within one standard deviation [9], indicating negligible $SU(3)$ flavor-breaking effects in the final state. Consequently, analyzing the mechanism underlying the significant deviation of the angular distribution parameter α for $\psi(3686)\to p\bar{p}$ from those for the $\psi(3686)\to n\bar{n}$ and $J/\psi\to p\bar{p}$ decays [10], within the quark model framework [6], is challenging. Current experimental analyses are limited to one-dimensional (1D) angular distributions and do not account for potential asymmetry in the data [9]. The accumulation of large $\psi(3686)$ data samples at BESIII highlights the requirement of conducting updated and more comprehensive measurements to clarify the underlying dynamics and to constrain theoretical models of baryon production in charmonium decays.

Extending the $1+\alpha\cos^2\theta$ parameterization of angular distribution in previous analyses, an improved measurement can be performed by analyzing the two-dimensional (2D) angular distribution in polar and azimuthal angles, incorporating the effects of transverse beam polarization in e^+e^- collisions [14]. Several studies have investigated the asymmetry phenomena in electron–positron annihilation into protons [15–16]. To advance our understanding, a comprehensive approach incorporating potential physical asymmetries in the polar angular distribution is required. Accounting for asymmetries arising from interference contributions from two-photon processes and backgrounds originating from initial-state–final-state radiation (ISR–FSR) interference is essential for extracting precise angular coefficients and for clarifying the underlying production dynamics.

II. ANALYSIS OF ANGULAR DISTRIBUTION

At the $\psi(3686)$ energy point in electron-positron annihilation experiments such as those conducted at BEPCII, the final state $p\bar{p}$ events can be produced through several processes, as illustrated in Fig. 1: resonant production via $\psi(3686)$, single-photon exchange, and two-photon exchange. Among these, the $\psi(3686)$ resonance dominates with a cross-section of approximately 1700 nb, while the single-photon process provides a secondary contribution. The intermediate Z-boson exchange is neglected here due to its off-shell suppression, which leads to negligible production at this energy. Although the two-photon process appears at the order of $\alpha^4_{\rm QED}$ and is negligible, its interference with the $\psi(3686)$ amplitude could introduce non-trivial asymmetries in the polar angular distribution. The asymmetries can be tested experimentally using available data.

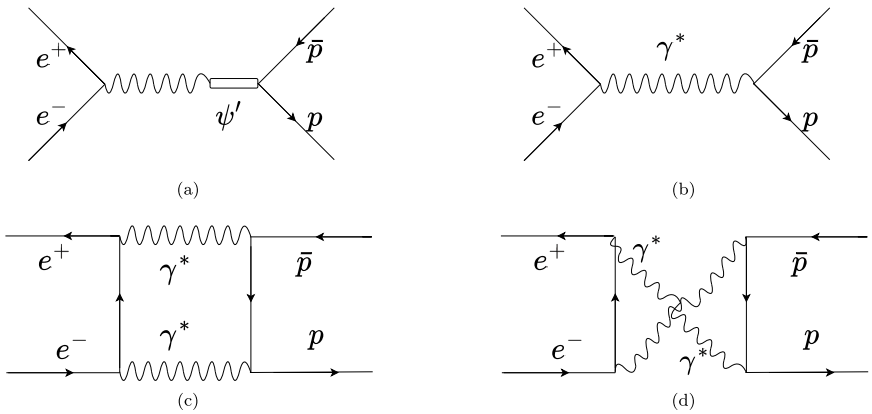

Fig. 1. Feynman diagrams of one (a,b) and two (c,d) virtual photon processes $e^+e^-\to\gamma^*/\psi(3686)$ or $\gamma^*\gamma^*\to p\bar{p}$.

Table 1. Measurements of branching fractions ($\mathcal{B}$) and angular distribution parameters (α) for $\psi(3686) \to p\bar{p}$ and $\psi(3686) \to n\bar{n}$ decays. The first and second uncertainties are statistical and systematic, respectively.

Source(Year)	Process	Branching Ratio $\mathcal{B}$	α parameter	Ref.
BES (2004)	$J/\psi \to p\bar{p}$	$(2.26 \pm 0.01 \pm 0.14) \times 10^{-3}$	$0.676 \pm 0.036 \pm 0.042$	[10]
BES (2012)	$J/\psi \to p\bar{p}$	$(2.112 \pm 0.004 \pm 0.031) \times 10^{-3}$	$0.595 \pm 0.012 \pm 0.015$	[11]
BES (2012)	$J/\psi \to n\bar{n}$	$(2.07 \pm 0.01 \pm 0.17) \times 10^{-3}$	$0.50 \pm 0.04 \pm 0.21$	[11]
BES (2007)	$\psi(3686) \to p\bar{p}$	$(3.36 \pm 0.09 \pm 0.25) \times 10^{-4}$	$0.85 \pm 0.24 \pm 0.04$	[12]
CLEO (2005)	$\psi(3686) \to p\bar{p}$	$(2.87 \pm 0.12 \pm 0.15) \times 10^{-4}$	α not reported	[13]
BESIII (2018)	$\psi(3686) \to p\bar{p}$	$(3.05 \pm 0.02 \pm 0.12) \times 10^{-4}$	$1.03 \pm 0.06 \pm 0.03$	[9]
BESIII (2018)	$\psi(3686) \to n\bar{n}$	$(3.06 \pm 0.06 \pm 0.14) \times 10^{-4}$	$0.68 \pm 0.12 \pm 0.11$	[9]

Experimentally, the $p\bar{p}$ final state is characterized by two angular observables: the polar angle θ and the azimuthal angle ϕ. The contributions from the aforementioned processes, including their coherent interference, can be described by a differential angular distribution that depends on both θ and ϕ. This distribution provides a sensitive probe to disentangle the resonant, single-photon, and two-photon components, as well as to test potential interference effects that may arise from transverse beam polarization or higher-order QED contributions. Such analyses enhance the precision of cross-section measurements and enable deeper investigations into the dynamics of baryon pair production near charmonium resonances.

In this section, we formulate the angular distribution for the resonant and single-photon processes by incorporating the beam transverse polarization. Subsequently, we extend the analysis to include the interference with the two-photon exchange process. Finally, we formulate the interference terms from ISR and FSR.

A. Beam transverse polarization

At BEPCII, the transverse polarization of electron and positron beams arises naturally owing to the Sokolov–Ternov effect [14]—a self-polarization mechanism where spin-flip synchrotron radiation during circulation in the storage ring leads to a gradual buildup of polarization perpendicular to the beam direction. This process results in a characteristic polarization P_T that increases with storage time, reaching significant levels away from depolarization resonances. The spin density matrix of beams can be described by [17]

$$\rho^- = \frac{1}{2}\begin{pmatrix} 1+P_z & P_T \\ P_T^* & 1-P_z \end{pmatrix} \quad \text{for } e^-,$$
$$\rho^+ = \frac{1}{2}\begin{pmatrix} 1+\bar{P}_z & P_T \\ P_T^* & 1-\bar{P}_z \end{pmatrix} \quad \text{for } e^+,$$

where P_z and $\bar{P}_z$ denote the longitudinal polarizations of the electron and positron, respectively. In the symmetric BEPCII configuration with transverse polarization only, $P_z = \bar{P}_z = 0$ and P_T is non-zero, leading to off-diagonal elements that modify angular distributions and enable new observables in baryon decay analyses.

At the BEPCII experiment, the evolution of beam transverse polarization is intrinsically linked to the storage ring's geometry and operational conditions. The polarization builds up naturally through the Sokolov–Ternov effect, with a characteristic time dependence described by $P_t = |P_T| = P_0(1 - e^{-t/\tau_0})$, where τ_0 depends on the ring radius and beam energy. A simplified numerical estimate indicates that, after about one hour of beam injection at the $\psi(3686)$ energy, the transverse polarization can reach approximately 28% [17]. This polarization can be experimentally measured offline using reference processes such as $e^+e^- \to \mu^+\mu^-$ and $\gamma\gamma$ production. The availability of transverse polarization introduces additional observables in the angular distribution of $p\bar{p}$ final states, enabling a deeper investigation into the underlying production mechanisms —particularly the origin of azimuthal asymmetries that may arise from interference between resonant and continuum amplitudes.

B. $e^+e^- \to \gamma^*/\psi(3686) \to p\bar{p}$

For the process $e^+e^- \to p\bar{p}$ via the intermediate states $\gamma^*/\psi(3686)$, its angular distribution can be written as

$$\frac{\mathrm{d}\sigma}{\mathrm{d}\cos\theta} \propto \sum_{\lambda_i,\lambda_i'} \rho^-_{\lambda_a,\lambda_a'} \rho^+_{\lambda_b,\lambda_b'} D^{1*}_{\lambda_a-\lambda_b,\lambda_c-\lambda_d}(\phi,\theta,0) \times D^1_{\lambda_a'-\lambda_b',\lambda_c-\lambda_d}(\phi,\theta,0) T^1_{\lambda_a,\lambda_b,\lambda_c,\lambda_d} T^{1*}_{\lambda_a',\lambda_b',\lambda_c,\lambda_d}, \quad (2)$$

where λ_a, $\lambda_a' = \pm 1/2$ and λ_b, $\lambda_b' = \pm 1/2$ denote the helicity values of the electron and positron, respectively. $\lambda_c = \pm 1/2$ and $\lambda_d = \pm 1/2$ denote the helicities of the proton and antiproton. $D^J_{m_1,m_2}$ represents the Wigner-D function in terms of the proton helicity angles θ and ϕ, and T^1 denotes the helicity amplitude. The process conserves the parity, leading to the symmetry relation $T^1_{-\lambda_a,-\lambda_b,-\lambda_c,-\lambda_d} = T^1_{\lambda_a,\lambda_b,\lambda_c,\lambda_d}$. Considering that the process $e^+e^- \to \gamma^*$ strictly obeys the helicity conservation rule, this leads to the heli-

city selection rule for e^+/e^-, which can be expressed using the Kronecker delta $\delta_{\lambda_a,-\lambda_b}$. Straightforward algebraic simplification yields

$$\frac{\mathrm{d}\sigma}{\mathrm{d}\cos\theta\mathrm{d}\phi} \propto 1+\alpha\cos^2\theta+\alpha P_t^2\sin^2\theta\cos 2\phi,$$

where α is the angular distribution parameter for proton within the region $\alpha\in[-1,1]$. Here the normalized relations, $|T^1_{1/2,-1/2,1/2,-1/2}|^2 = (1+\alpha)/2$ and $|T^1_{1/2,-1/2,1/2,1/2}|^2 = (1-\alpha)/4$, are used.

C. Interference with two-photon process

To account for the potentially asymmetric angular distribution of the proton, we consider the interference between processes involving $\psi(3686)$ and two-photon contributions. The proton distribution from $\psi(3686)$ decay yields a symmetric profile, corresponding to the S- and D-wave components of the proton, whereas the two-photon process also comprises contributions from partial waves with $L=1,3$. Interference between these terms therefore leads to an asymmetric distribution. In this analysis only P-wave contribution is considered. The amplitudes for processes (a) and (c) in Fig. 1 can be uniformly expressed as

$$\mathcal{A}_{a/c}(\lambda_a,\lambda_b,\lambda_c,\lambda_d) = \frac{1}{4\pi}\sum_{J_{a/c}}(2J_{a/c}+1) \times D^{J_{a/c}*}_{\lambda_a-\lambda_b,\lambda_c-\lambda_d}(\phi,\theta,0)T^{J_{a/c}}_{\lambda_a,\lambda_b,\lambda_c,\lambda_d}, \quad (3)$$

where $J_{a/c}$ represents the spin of the intermediate state. For the $\psi(3686)$ process, we take $J_a=1$. In the case of the two-photon process, three spin configurations are possible: $J_c=0,1,2$. The helicity selection rule forbids simultaneous coupling of one and two photons of $J_c=0$ system to the e^+e^- beams, which cancels the interference contribution. For the $J_c=1$ configuration, C-parity conservation results in only one non-zero helicity amplitude, $T_{1/2,-1/2,1/2,-1/2}$, yielding a symmetric distribution of order $\alpha^4_{\rm QED}$, which can be neglected. Thus, we only consider the interference term of the case $J_c=2$ with resonance, at level of $\alpha^2_{\rm QED}$ order. Then we have the interference contribution $\mathcal{I}_{ac}\propto\sum_{\lambda_i}\rho^-_{\lambda_a,\lambda'_a}\rho^+_{\lambda_b,\lambda'_b}\mathrm{Re}(\mathcal{A}_a\mathcal{A}^*_c)$, and

$$\mathcal{A}_a\mathcal{A}^*_c \propto D^{1*}_{\lambda_a-\lambda_b,\lambda_c-\lambda_d}(\phi,\theta,0)D^2_{\lambda'_a-\lambda'_b,\lambda_c-\lambda_d}(\phi,\theta,0) \times T^1_{\lambda_a,\lambda_b,\lambda_c,\lambda_d}T^{2*}_{\lambda'_a,\lambda'_b,\lambda_c,\lambda_d}. \quad (4)$$

Using the parity-conserved relations, $T^2_{-\lambda_a,-\lambda_b,-\lambda_c,-\lambda_d} = T^2_{\lambda_a,\lambda_b,\lambda_c,\lambda_d}$, the following reduced formula is obtained:

$$\frac{\mathrm{d}\mathcal{I}_{ac}}{\mathrm{d}\cos\theta\mathrm{d}\phi} \propto \cos\theta\left[A\cdot[\cos^2\theta+P_t^2\cos(2\phi)\sin^2\theta]-B\cdot\sin^2\theta\right],$$

$$\text{with}\quad A = 8\sqrt{2}\sqrt{1+\alpha}\cos\left(\frac{1+\alpha}{2}+\beta\right)H^2_{\frac12,-\frac12,\frac12,-\frac12}, \quad (5)$$

$$B = 8\sqrt{3}\sqrt{|\alpha-1|}\left[-1+P_t^2\cos(2\phi)\right] \times\cos\left(\frac{3}{2}(\alpha-1)\right)H^2_{\frac12,-\frac12,\frac12,\frac12}, \quad (6)$$

where β is the phase angle difference between $T^1_{1/2,-1/2,1/2,1/2}$ and $T^1_{1/2,-1/2,1/2,-1/2}$, and α is the angular distribution parameter of the proton. Here, we treat H^2 as a real number, based on the following consideration: photon coupling with charged particles occurs via $(ie)^2$ and both the photon and proton are zero-width particles, leading to a real amplitude. A previously reported numerical investigation [18] shows that the form factor for photon–proton coupling has a negligible imaginary part, which justifies the use of a real-amplitude approximation.

If ϕ is integrated out, then we obtain a reduced distribution [15, 18]:

$$\frac{\mathrm{d}\mathcal{I}_{ac}}{\mathrm{d}\cos\theta} \propto B\cos\theta+(A-B)\cos^3\theta, \text{ with}$$
$$A = 8\sqrt{2}\sqrt{1+\alpha}\cos\left(\frac{1+\alpha}{2}+\beta\right)H^2_{\frac12,-\frac12,\frac12,-\frac12},$$
$$B = 8\sqrt{3}\sqrt{|\alpha-1|}\cos\left(\frac{3}{2}(\alpha-1)\right)H^2_{\frac12,-\frac12,\frac12,\frac12}. \quad (7)$$

The asymmetry distribution is plotted in Fig. 2 for the parameter choice $\alpha=1$, $\beta=0$ and is displayed in arbitrary units.

D. ISR–FSR interference

The corrections from ISR and FSR have been extensively studied in quantum electrodynamics. Calculations

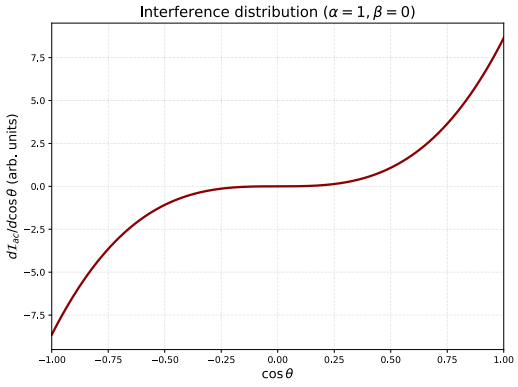

Fig. 2. (color online) Asymmetric proton angular distribution resulting from the interference between resonance and two-photon processes.

show that the photon radiation from charged particles is concentrated near the direction of the particle's motion, decreases rapidly as the angle increases, and the radiation probability is inversely proportional to the square of the charged particle's mass. The higher the energy of the radiated photon, the lower the probability of its emission.

In ISR, mostly soft photons are produced along the beam direction. By contrast, in FSR, the photons radiated by protons and antiprotons are mainly emitted along their respective directions of motion. Because their energies are mostly below the sensitivity threshold of photon detectors, they may not be detected. Such undetected FSR processes have the same final observed state as that of the signal channel and thus form an important type of background. The tree level of ISR–FSR diagram is shown in Fig. 3.

Although the probability of FSR from protons (antiprotons) is considerably smaller than that of ISR, the interference between them can lead to an asymmetric angular distribution. This asymmetry is observed because, in ISR, the $p\bar{p}$ system has a parity of 1^- and is in a state represented by the superposition of S- and D-wave states, whereas in FSR, the $p\bar{p}$ system is in a P-wave state. The interference between states of different parity can produce an asymmetric angular distribution. This asymmetric profile has been found for the process reported in a previous study [16].

To investigate the contribution of the ISR–FSR interference to the asymmetry, we compute the interference term between diagrams (a) and (b) in Fig. 3, which can be written as $I_{12} \propto 2\mathcal{R}e\left(\rho^+\rho^-\mathcal{M}_1\mathcal{M}_2^*\right)$. Here ρ^+ and ρ^- denote the spin density matrices of the positron and electron, respectively, while $\mathcal{M}_1$ and $\mathcal{M}_2$ represent the amplitudes corresponding to diagrams (a) and (b) in Fig. 3.

For diagram (a) the amplitude reads

$$\begin{aligned}\mathcal{M}_1 \sim & D^1_{\lambda'_+-\lambda_-,\,\lambda_p-\lambda_{\bar{p}}}(\phi,\theta,0)\,D^{\frac{1}{2}}_{\lambda'_+,\,\lambda_+-\lambda_\gamma}(\phi_1,\theta_1,0)\\ & \times H_{\lambda'_+,\lambda_-,\lambda_p,\lambda_{\bar{p}}}\,G_{\lambda_+,\lambda_\gamma},\end{aligned} \tag{8}$$

where λ_+, λ_-, λ_p, and $\lambda_{\bar{p}}$ are the helicities of the positron, electron, proton, and antiproton, respectively. The factor $G_{\lambda_+,\lambda_\gamma}$ is the helicity amplitude for the subprocess $e^+ \to \gamma e^+$, described by the helicity angles (ϕ_1,θ_1). The quantity $H_{\lambda'_+,\lambda_-,\lambda_p,\lambda_{\bar{p}}}$ denotes the helicity amplitude for the coupling of the e^+e^- pair to the $p\bar{p}$ system.

For diagram (b), the amplitude is

$$\begin{aligned}\mathcal{M}_2 \sim & D^1_{\lambda_+-\lambda_-,\,\lambda'_p-\lambda_{\bar{p}}}(\phi,\theta,0)\,D^{\frac{1}{2}}_{\lambda'_p,\,\lambda_p-\lambda_\gamma}(\phi_2,\theta_2,0)\\ & \times H_{\lambda_+,\lambda_-,\lambda'_p,\lambda_{\bar{p}}}\,F_{\lambda_p,\lambda_\gamma},\end{aligned} \tag{9}$$

where $F_{\lambda_p,\lambda_\gamma}$ is the helicity amplitude for the radiation $p \to \gamma p$ with helicity angles (ϕ_2,θ_2), and $H_{\lambda_+,\lambda_-,\lambda'_p,\lambda_{\bar{p}}}$ describes the $e^+e^- \to p\bar{p}$ vertex.

Considering both ISR and the two FSR possibilities for the cases in which the photon is emitted from either the proton or the antiproton, the interference contribution to the cross-section can be expressed as

$$\sigma_{\text{ISR–FSR}} \propto 2\,\text{Re}\Big[\rho^+\rho^-\mathcal{M}_1\left(\mathcal{M}_2^* + \mathcal{M}_2^*([\theta_2,\phi_2] \to [\theta_3,\phi_3])\right)\Big], \tag{10}$$

where the replacement $[\theta_2,\phi_2] \to [\theta_3,\phi_3]$ indicates that the FSR photon is emitted from the antiproton, with corresponding helicity angles θ_3,ϕ_3. Events in which the ISR or FSR photon escapes detection (because it is soft or collinear) lead to the same visible final state as the that of the signal channel $e^+e^- \to p\bar{p}$. Therefore, such configurations constitute an irreducible background. In the present study, these contributions are treated by integrating over the unobserved photon angles.

If the angles for the ISR (FSR) photons are integrated out, then the angular distribution is obtained as

$$\begin{aligned}\frac{\mathrm{d}\sigma_{\text{ISR–FSR}}}{\mathrm{d}\cos\theta\,\mathrm{d}\phi} \propto & 4\Big(6 + 6\cos(2\theta) - \sqrt{2}\sin\theta\\ & + 6P_t^2\cos(2\phi)\sin\theta\Big(\sqrt{2}\sin^2\left(\frac{\theta}{2}\right) + 2\sin\theta\Big)\\ & + \cos\theta\Big(4 + 3\sqrt{2}\sin\theta\Big)\Big)\alpha - 2\Big(4\sqrt{2}\cos\theta + \sqrt{2}\cos(2\theta)\\ & + 2\sin\theta\Big(12 + \sqrt{2}P_t^2\cos(2\phi)\sin\theta\Big)\Big)\sqrt{1-\alpha^2}\\ & + 2\Big(24 + 8\cos\theta + 8\sqrt{2}P_t^2\cos\left(\frac{\theta}{2}\right)\cos(2\phi)\sin^3\left(\frac{\theta}{2}\right)\\ & - 6\sqrt{2}\sin\theta + \sqrt{2}\sin(2\theta) + 5\sqrt{2-2\alpha^2}\Big),\end{aligned} \tag{11}$$

where P_t and α are the beam transverse polarization and angular distribution parameter of the proton, respectively.

If ϕ is integrated out, then

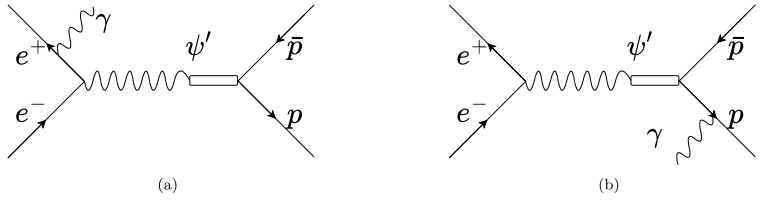

Fig. 3. Tree level of Feynman diagrams for ISR (a), FSR, (b) processes $e^+e^- \to \psi(3686) \to p\bar{p}$.

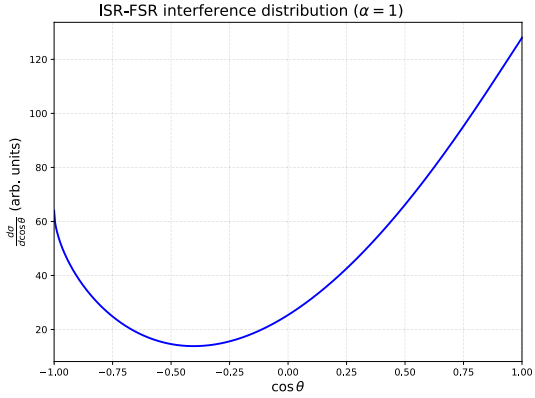

Fig. 4. (color online) Asymmetric proton angular distribution resulting from the interference between ISR and FSR processes.

$$\begin{aligned}\frac{\mathrm{d}\sigma_{\mathrm{ISR-FSR}}}{\mathrm{d}\cos\theta} \propto\ & 4\Big(6+6\cos(2\theta)-\sqrt{2}\sin\theta+4\cos\theta \\ & +3\sqrt{2}\sin\theta\cos\theta\Big)\alpha \\ & -2\Big(4\sqrt{2}\cos\theta+\sqrt{2}\cos(2\theta)+24\sin\theta\Big)\sqrt{1-\alpha^2} \\ & +2\Big(24+8\cos\theta-6\sqrt{2}\sin\theta+\sqrt{2}\sin(2\theta) \\ & +5\sqrt{2}\sqrt{1-\alpha^2}\Big).\end{aligned} \tag{12}$$

In Fig. 4, the asymmetry distribution is plotted for the $\alpha = 1$ parameter choice and is displayed in arbitrary units.

III. UPDATE ANALYSIS OF $e^+e^- \to p\bar{p}$

A. Updating the fit to the measured proton $\cos\theta$ distribution

The angular distributions for $\psi(3686) \to p\bar{p}$ and $n\bar{n}$ were previously measured by the BESIII collaboration [9] using 1.07×10^8 $\psi(3686)$ events. In this previous analysis, the angular distribution was described by $1+\alpha\cos^2\theta$, and the possibility of a forward–backward asymmetry was explored by introducing an odd $\cos\theta$ contribution into the angular distribution, parametrized as $1+\beta\cos\theta+\alpha\cos^2\theta$. Although the anomalous term was zero, $\beta_{n\bar{n}} = 0.04\pm0.05$, and $\beta_{p\bar{p}} = 0.01\pm0.02$, its physical origin remained unspecified, and the treatment should be understood beyond the empirical asymmetry. Moreover, this analysis did not account for the background from ISR–FSR interference. To properly account for the two-photon interference asymmetry and incorporate the ISR–FSR interference background, we performed a renewed fit to the angular distribution incorporating the asymmetry sources.

The fitting is performed using the maximum likelihood (ML) method. The likelihood function $\mathcal{L}$ is defined as

$$\mathcal{L}(\vec{p}) = \prod_{i=1}^{n} P\left(y_i \,|\, \frac{\mathrm{d}\sigma^{\mathrm{tot}}}{\mathrm{d}\cos\theta}(\theta_i;\vec{p}),\sigma_i^-,\sigma_i^+\right), \tag{13}$$

where y_i is the observed number of events at θ_i; $\frac{\mathrm{d}\sigma^{\mathrm{tot}}}{\mathrm{d}\cos\theta}(\theta_i;\vec{p})$ is the theoretical prediction evaluated with the parameter $\vec{p}$; and σ_i^- and σ_i^+ are the lower and upper uncertainties in the measurement, respectively. The probability density function P is constructed using a Gaussian function.

The fitting procedure yields the optimal parameter estimates by minimizing the negative log-likelihood:

$$-\ln\mathcal{L}(\vec{p}) = -\sum_{i=1}^{n}\ln P\left(y_i \,|\, \frac{\mathrm{d}\sigma^{\mathrm{tot}}}{\mathrm{d}\cos\theta}(\theta_i;\vec{p}),\sigma_i^-,\sigma_i^+\right). \tag{14}$$

Because only a 1D distribution in $\cos\theta$ is available in the previously reported analysis [9], the theoretical angular distribution function $\frac{\mathrm{d}\sigma^{\mathrm{tot}}}{\mathrm{d}\cos\theta}$ is defined by integrating out φ:

$$\frac{\mathrm{d}\sigma_p^{\mathrm{tot}}}{\mathrm{d}\cos\theta} = N\epsilon(\theta)\left(\frac{\mathrm{d}\sigma}{\mathrm{d}\cos\theta}+\frac{\mathrm{d}\mathcal{I}_{ac}}{\mathrm{d}\cos\theta}+c_1\frac{\mathrm{d}\sigma_{\mathrm{ISR-FSR}}}{\mathrm{d}\cos\theta}\right), \tag{15}$$

where N is a normalization factor, $\epsilon(\theta)$ represents the efficiency correction curve adopted from the experimental analysis [9], and c_1 is a fit parameter scaling the contribution from ISR–FSR.

The measured angular parameter α is $1.03\pm0.06\pm0.03$ [9] with the $1+\alpha\cos^2\theta$ parameterization. Subsequently, we perform a new ML fit to this reported angular distribution to test the validity of our proposed formalism. In the ML fitting process, we treat $H^2_{\frac{1}{2},-\frac{1}{2},\frac{1}{2},-\frac{1}{2}}$ and $H^2_{\frac{1}{2},-\frac{1}{2},\frac{1}{2},\frac{1}{2}}$ as real parameters and float $H^2_{\frac{1}{2},-\frac{1}{2},\frac{1}{2},-\frac{1}{2}}$, $H^2_{\frac{1}{2},-\frac{1}{2},\frac{1}{2},\frac{1}{2}}$, N, c_1, α, and β. The results are shown in Fig. 5, and the fitted values of the main parameters are summarized in Table 2.

Our fitted angular parameter for the proton, $\alpha = 1.00\pm0.03$, is consistent with the previously reported value of $\alpha = 1.03\pm0.06\pm0.03$ within one standard deviation. With the fitted parameters, we plot the ϕ distribution as shown in Fig. 6. A distinct feature is the deviation of the $\psi(3686)$ production distribution from the phase-space distribution; it exhibits a $\sin(2\phi)$ modulation, whereas the phase space is flat. The interference contributions from the resonance and two-photon process are relatively small but non-trivial. By contrast, the ISR–FSR interference background is negligible. To reveal the transverse polarization and the interference behavior between

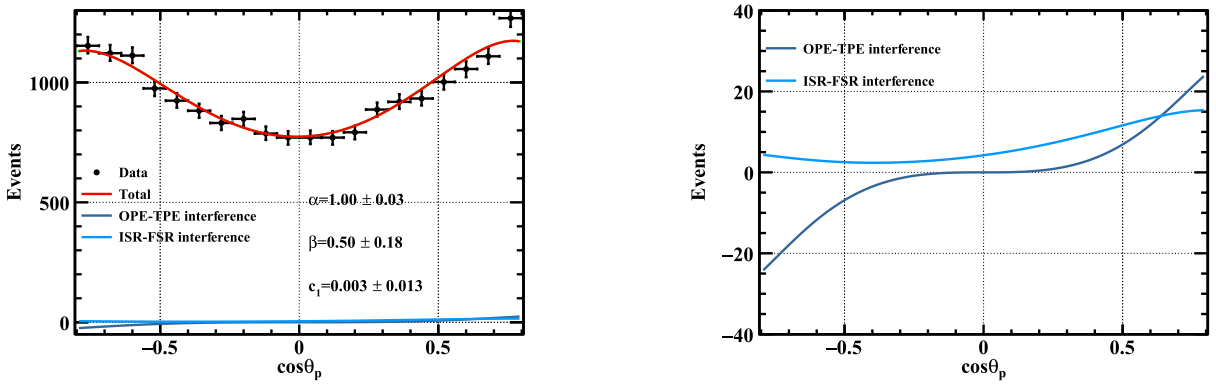

Fig. 5. (color online) Plot of $\cos\theta_p$ distribution. The contribution of the interference with two-photon exchange process is shown by a azure line. The contribution of ISR and fFSR interference is shown by a light blue line. The total PDF is shown by a red line. (b) Distributions of the interference terms.

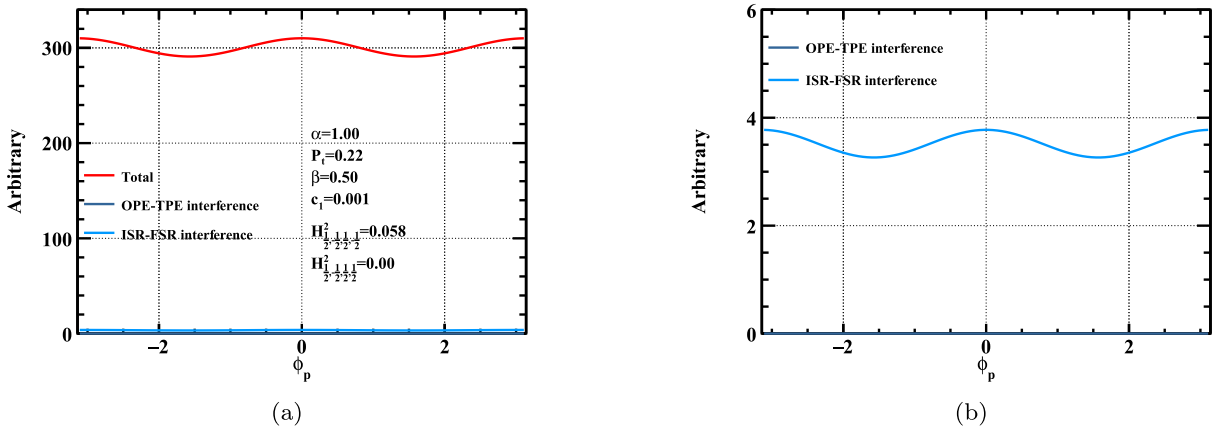

Fig. 6. (color online) Plot of expected ϕ_p distribution at $\alpha = 1.00$, $P_t = 0.22$, $\beta = 0.50$, $c_1 = 0.003$, $H^2_{1/2,-1/2,1/2,-1/2} = 0.058$, and $H^2_{1/2,-1/2,1/2,1/2} = 0.0$. (b) Distributions of the interference terms.

Table 2. Parameter results of the proton angular distribution fit.

Parameter	Value
α	1.00 ± 0.03
β	0.50 ± 0.18
$H^2_{1/2,-1/2,1/2,-1/2}$	0.058 ± 0.072
$H^2_{1/2,-1/2,1/2,1/2}$	0.00 ± 0.01

the resonance and two-photon processes, a 2D analysis of the polar and azimuthal angles of the nucleon should be performed. We anticipate the realization of this approach in future data analysis.

B. Sensitivity of P_t measurement

To evaluate the sensitivity of P_t measurement, we generate approximately 0.17 million toy Monte Carlo (MC) events using the amplitude model for the $\psi(3686) \to p\bar{p}$ decay at each P_t value of P_t = 0.1, 0.2, 0.4, 0.6, 0.8. The other parameters are fixed as $\alpha = 1.00$, $\beta = 0.50$, $c_1 = 0.003$, $H^2_{1/2,-1/2,1/2,-1/2} = 0.058$, and $H^2_{1/2,-1/2,1/2,1/2} = 0.0$. To examine the sensitivity to the number of events, multiple samples are prepared by sampling randomly from the 0.17 million toy MC events. Additionally, approximately 0.38 million phase-space MC events are generated for calculating the normalization factor in the likelihood function.

The 2D differential cross-section is defined as

$$\frac{\mathrm{d}\sigma^{\rm tot}}{\mathrm{d}\cos\theta\mathrm{d}\varphi} = \frac{\mathrm{d}\sigma}{\mathrm{d}\cos\theta\mathrm{d}\varphi} + \frac{\mathrm{d}\mathcal{I}_{ac}}{\mathrm{d}\cos\theta\mathrm{d}\varphi} + c_1\frac{\mathrm{d}\sigma_{\rm ISR-FSR}}{\mathrm{d}\cos\theta\mathrm{d}\varphi}, \tag{16}$$

The likelihood function for i-th event is defined as

$$\mathcal{L}^i(\cos\theta_i,\phi_i|\alpha,P_t,\beta,c_1,H^2_{\frac{1}{2},-\frac{1}{2},\frac{1}{2},-\frac{1}{2}},H^2_{\frac{1}{2},-\frac{1}{2},\frac{1}{2},\frac{1}{2}}) = \frac{\mathrm{d}\sigma^{\rm tot}/\mathrm{d}\cos\theta_i\mathrm{d}\varphi_i}{\sigma^{\rm tot}}, \tag{17}$$

where the normalization factor $\sigma^{\rm tot}$ is calculated using the

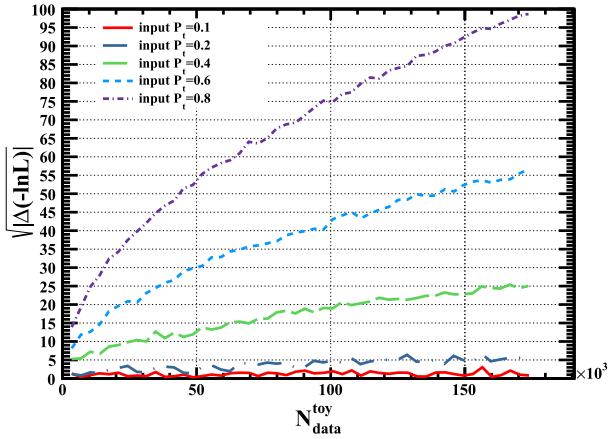

Fig. 7. (color online) P_t significance as a function of the number of toy sample events and the input P_t value.

MC method as $\sigma^{\rm tot} = \frac{1}{N_{\rm MC}}\sum_i^{N_{\rm MC}} \frac{{\rm d}\sigma^{\rm tot}}{{\rm d}\cos\theta_i {\rm d}\varphi_i}$ ($N_{\rm MC}$ is the number of phase-space MC events). Instead, we minimize the object function for the $N_{\rm dt}$ events

$$-\ln L = -\sum_i^{N_{\rm dt}} \ln \mathcal{L}^i, \tag{18}$$

using the TMinuit package [19]. The statistical significance of the measured P_t signal is estimated by comparing the differences in the log-likelihood values ($\Delta(-\ln L)$) with and without the P_t parameter. The resulting significance for the P_t parameter is estimated using $\sqrt{|\Delta(-\ln L)|}$, and then, it is plotted as a function of the number of events for different P_t values.

As shown in Fig. 7, a significance of 5σ can be achieved with only approximately 0.1 million events when $P_t \geq 0.2$. Given that BESIII has accumulated 2712.4 million $\psi(3686)$ events, approximately 0.5 million $\psi(3686) \to p\bar{p}$ events can be selected. This sample allows precise measurement of the transverse beam polarization at BEPCII, which is theoretically expected to reach ~0.28 [17] after 1 h of beam energy injection.

IV. SUMMARY AND OUTLOOK

This paper presents an updated analysis of the angular distribution in the $\psi(3686) \to p\bar{p}$ decay. This analysis, explicitly incorporating the effects of transverse beam polarization and revealing potential physical sources of asymmetry, extends beyond the traditional $1+\alpha\cos^2\theta$ parameterization. The analysis is focused on two key contributions: the interference between the resonant $\psi(3686)$ amplitude and the two-photon exchange continuum, and the background from ISR–FSR interference. An ML fit to the 1D $\cos\theta$ distribution yields an angular parameter $\alpha = 1.00 \pm 0.03$, which is consistent with the previous BESIII measurement. The fitted contributions from the two-photon interference and the ISR–FSR background are found to be consistent with zero within uncertainties, while their inclusion is essential for a complete description of the angular distribution. We have also estimated the statistical significance of P_t measurement using the generated toy MC events. A significance of 5σ can be achieved with approximately 0.1 million events when $P_t \geq 0.2$. Notably, incorporating transverse polarization results in the prediction of a distinct $\sin(2\phi)$ modulation in the azimuthal distribution; this feature clearly deviates from the expected flat phase-space.

Our study highlights the limitations of 1D angular analyses and underscores the importance of a full 2D $(\cos\theta, \phi)$ approach to disentangle the associated complex dynamics. The observed $\sin(2\phi)$ modulation, directly linked to transverse beam polarization, serves as a new observable sensitive to the interference between the resonant and non-resonant amplitudes. Future analyses with higher statistics should implement such a 2D angular fit to allow for a more precise and simultaneous extraction of the polar asymmetry parameter α and ϕ-modulation coefficients as well as to enable a direct constraint on the transverse polarization degree P_t from the baryon decay data itself. Such an analysis would enable cross-assessment with other calibration processes such as $e^+e^- \to \mu^+\mu^-$.

With the continued accumulation of $\psi(3686)$ data at BESIII and the potential for dedicated runs with enhanced beam polarization, sensitive measurements can be performed in the future to precisely determine the helicity amplitudes governing the two-photon process. The corresponding results will offer deeper insights into the interplay between QCD-driven resonance decays and QED continuum processes in the timelike region. This comprehensive angular analysis provides critical insights for comprehensively understanding charmonium decays to baryon–antibaryon pairs.

References

[1] M. Ablikim *et al.* (BESIII Collaboration), Phys. Rev. Lett. **124**, 042001 (2020)

[2] M. Ablikim *et al.* (BESIII Collaboration), Phys. Rev. Lett. **130**, 151905 (2023)

[3] G. Huang *et al.* (BESIII Collaboration), Natl. Sci. Rev. **8**, 187 (2021)

[4] M. Ablikim *et al.* (BESIII Collaboration), Nature Phys. **17**, 1200 (2021)

[5] J. P. Lees *et al.* (BABAR Collaboration), Phys. Rev. D **87**, 092005 (2013)

[6] R. G. Ping, H. C. Chiang, and B. S. Zou, Phys. Rev. D **66**, 054020 (2002)

[7] N. Kivel, Eur. Phys. J. A **56**, 64 (2020)
[8] A. Cieply, Int. J. Mod. Phys. A **20**, 1859 (2005)
[9] M. Ablikim *et al*. (BESIII Collaboration), Phys. Rev. D **98**, 032006 (2018)
[10] J. Z. Bai *et al*. (BESIII Collaboration), Phys. Lett. B **591**, 42 (2004)
[11] M. Ablikim *et al*. (BESIII Collaboration), Phys. Rev. D **86**, 032014 (2012)
[12] M. Ablikim *et al*. (BESIII Collaboration), Phys. Lett. B **648**, 149 (2007)
[13] T. K. Pedlar *et al*. (CLEO Collaboration), Phys. Rev. D **72**, 051108 (2005)
[14] A. A. Sokolov and I. M. Ternov, Sov. Phys. Dokl. Akad. Nauk SSSR **153**, 1052 (1963)
[15] L. Xia, arXiv: 2508.12812
[16] H. Czyz, A. Grzelinska, J. H. Kuhn *et al*., Eur. Phys. J. C **33**, 333 (2004)
[17] X. Cao, Y. T. Liang, and R. G. Ping, Phys. Rev. D **110**, 014035 (2024)
[18] D. Y. Chen, H. Q. Zhou, and Y. B. Dong, Phys. Rev. C **78**, 045208 (2008)
[19] F. James, *Function Minimization and Error Analysis*, CERNLIB D506, (1998)